A mid-infrared diagnostic for benzene using a tunable difference-frequency-generation laser

Proceedings of the Combustion Institute (Accepted manuscript)

DOI: https://doi.org/10.1016/j.proci.2020.06.382

A Mid-Infrared Diagnostic for Benzene Using a Tunable Difference-Frequency-Generation Laser

Mohammad K. Shakfa[1], Mhanna Mhanna[1], Hanfeng Jin[1], Dapeng Liu[1], Khalil Djebbi[1], Marco Marangoni[2], Aamir Farooq[1]*

[1]King Abdullah University of Science and Technology (KAUST), Clean Combustion Research Center, Physical Sciences and Engineering Division, Thuwal 23955-6900, Saudi Arabia

[2]Dipartimento di Fisica - Politecnico di Milano and IFN-CNR, Via Gaetano Previati 1/C, 23900 Lecco, Italy

Colloquium: Diagnostics

Word Count:

The total length of paper: 6048 words (Method 1)

Main text: 3362 words

Equations: 160 words

References: 647 words

Tables: 0 words

Figures and Captions: 1879 words

Abstract

Benzene is a very important molecule in a variety of industrial, environmental, and chemical systems. In combustion, benzene plays an essential role in the formation and growth of polycyclic aromatic hydrocarbons and soot. In this work, a new laser-based diagnostic is presented to make quantitative, interference-free, and sensitive measurements of benzene in the mid-IR region. The diagnostic is based on a widely tunable difference-frequency-generation (DFG) laser system. We developed this laser source to emit in the mid-IR between 666.54 cm^{-1} and 790.76 cm^{-1} as a result of the DFG process between an external-cavity quantum-cascade-laser and a CO_2 gas laser in a nonlinear, orientation-patterned GaAs crystal. Benzene measurements were carried out at the peak (673.94 cm^{-1}) of the Q-branch of the ν_{11} vibrational band of benzene. The absorption cross-section of benzene was measured over a range of pressures (4.44 mbar to 1.158 bar) at room temperature. The temperature dependence of the absorption cross-sections was studied behind reflected shock waves over 553–1473 K. The diagnostic was demonstrated in a high-temperature reactive experiment of benzene formation from propargyl radicals. The new diagnostic will prove highly beneficial for high-temperature studies of benzene formation and consumption kinetics.

Keywords: *Benzene; PAH formation; Absorption cross-section; Shock tube; Difference frequency generation.*

1. Introduction

Optical diagnostic techniques have been a powerful tool for combustion research and development. These techniques provide the possibility of sensitive, non-intrusive, in-situ detection of gaseous chemical substances [1]. In particular, laser absorption spectroscopy has been of high interest since it offers quantitative, species-specific measurements of temperature, pressure, and composition of chemical species in scientific, industrial, and environmental applications [2]. The combination of laser absorption spectroscopy and shock tubes has provided unique experimental capabilities to understand and develop chemical kinetics at high temperatures and pressures [2,3]. Beside shock tubes, laser absorption spectroscopy has been applied in a variety of combustion systems, e.g., internal combustion engines [4] and pulse detonation engines [5].

The development of new laser sources, especially in the mid-infrared (MIR) spectral range, has drawn high interest in recent years for combustion diagnostics. The major motivation for this is the fact that many gaseous chemical species of interest in combustion, e.g., CO, CO_2, H_2O, NO_x, hydrocarbons, show strong fundamental ro-vibrational absorption bands in the MIR spectral range. For example, the strongest absorption bands of the aromatic hydrocarbons of BTX family (benzene, toluene, and xylene isomers) lie in the wavenumber range between 666 cm^{-1} and 801 cm^{-1} [6]. Light absorption by these MIR bands can be uniquely exploited as a nearly universal tool for high-sensitivity sensing of gaseous chemical species. Consequently, tunable laser sources in the MIR spectral range have been of high demand for a variety of applications, including optical diagnostics for combustion and chemical kinetics studies. Quantum-cascade-lasers (QCLs) can be used to access a wide range of MIR wavelengths with high performance in terms of laser line-width and laser output power [7–9]. However, they do not offer broad tunability and are not available at wavelengths longer than ~12 μm (continuous- wave mode) or ~14 μm (pulsed mode). In contrast, nonlinear frequency conversion based laser sources offer a broad tunability and can be designed to target specific wavelength regions [10].

The main nonlinear frequency conversion laser sources are based on optical parametric oscillator and difference-frequency generation principles [11].

Benzene has been the subject of numerous theoretical and experimental works. Benzene is the simplest aromatic hydrocarbon and is one of the primary intermediates formed during the combustion of higher aromatics [12,13]. Furthermore, the chemistry of benzene at high temperatures has a significant role in the formation of larger polycyclic aromatic hydrocarbon (PAH) molecules [14–16]. The recombination of propargyl radicals to form benzene is a key pathway to the aromatic chain. The molecular structure of benzene has been widely studied using optical spectroscopy techniques, such as Raman spectroscopy and FTIR (Fourier-transform infrared spectroscopy) [17–19]. Laser-based sensing of benzene has been reported in the MIR at the wavenumbers of ~670 cm^{-1} [20], 676.6 cm^{-1} [21], 1012–1063 cm^{-1} [22,23], ~1025 [20], ~1943 cm^{-1} [24], ~1953 cm^{-1} [24], 3033.98–3089.28 cm^{-1} [25], and ~3043.8 cm^{-1} [26]. Benzene has also been also studied in the ultraviolet (UV) spectral range [25, 26]. In this context, benzene cross-section has been reported in the UV range at room temperature [28] and at high temperatures (690–1900 K) from shock tube experiments [27].

The strongest vibrational feature of benzene in the mid-IR range is the Q-branch of the ν_{11} vibrational band near 674 cm^{-1} (~14.84 μm). Apart from a room-temperature work [21], to the best of our knowledge, there have been no previous efforts in accessing this strong absorption of benzene for high-temperature studies. Likewise, high-temperature absorption cross-section of benzene has not been reported previously in this wavelength region, i.e., around 674 cm^{-1}. Here, we applied a tunable difference-frequency-generation (DFG) laser system to design a new diagnostic for interference-free and sensitive measurements of benzene in combustion environments.

2. Experimental details

2.1. Tunable mid-infrared DFG laser

Figure. 1(a) shows a schematic of the experimental setup for the DFG laser diagnostic. The pump beam was provided by an external-cavity quantum cascade laser (EC-QCL, Daylight Solutions) with single-

mode emission in the 1749.97–1820.03 cm^{-1} spectral range. An optical isolator (OI, Innovative Photonics) was used to suppress any optical feedback (mainly from the facets of the OP-GaAs crystal) that may damage the EC-QCL. The signal beam came from a CO_2 gas laser (Access Lasers, L20GD), non-continuously tunable between 920.81 cm^{-1} and 1083.42 cm^{-1}. This laser was operated in pulse mode with optical power up to 10 W at its most intense lines.

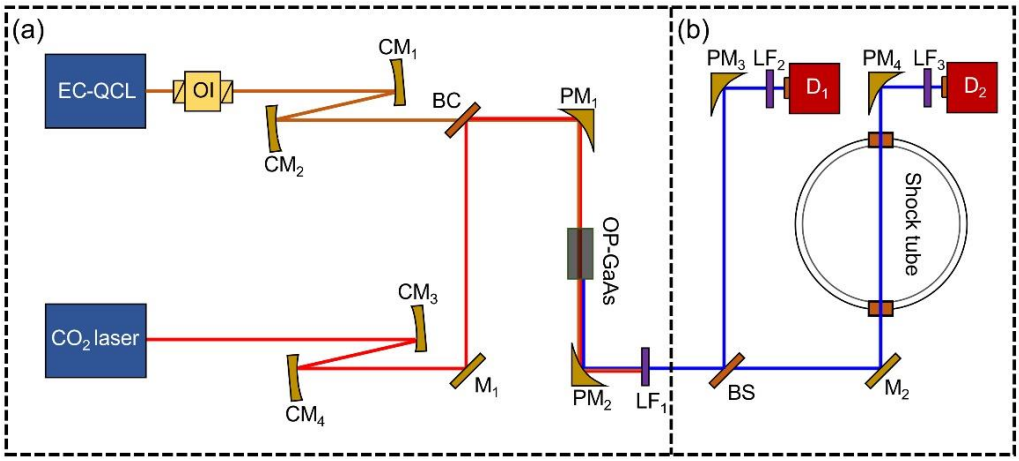

Fig. 1. Schematic drawing of (a) the DFG laser setup and (b) the cross-section of the shock tube. EC-QCL: external-cavity quantum cascade laser; OI: optical isolator; CM: concave mirror; BC: beam combiner; PM: parabolic mirror; M: mirror (flat); OP-GaAa: orientation-patterned GaAs crystal; LF: long-pass filter; BS: beam splitter; D: detector.

We used two sets of concave mirrors to optimize the beam waists of the pump and signal lasers inside the OP-GaAs crystal (BAE Systems Inc.) to maximize the DFG efficiency. The pump and signal laser beams were aligned through a beam combiner and focused onto the anti-reflection-coated OP-GaAs crystal by a parabolic mirror (PM). A second PM was used to collect the idler laser after the OP-GaAs crystal. A long-pass filter was placed after PM_2 to filter out both the pump and signal wavelengths. The DFG laser beam was split using a ZnSe beam splitter in two beams, as shown in Fig. 1(b). The *reflected* beam was directly focused onto a liquid-nitrogen-cooled HgCdTe detector (D_1, Infrared Associates Inc.) using PM_3, while the *transmitted* beam was aligned through the shock-tube via coated ZnSe windows and then focused onto another similar HgCdTe detector (D_2) using PM_4. A long-pass filter was installed in front of each detector to reduce optical noise and minimize thermal signal from the hot gases in the shock tube. This dual-beam configuration allows us to eliminate noise coming

from laser intensity fluctuations. In particular, the ratio between the intensity of the *transmitted* laser beam and the intensity of the *reflected* one is obtained when the shock tube is vacuumed. Then, we used this intensity ratio (R_{int}) to normalize the laser signal of both detectors, D_1 and D_2, when analyzing the results of the measurements to obtain benzene absorbance.

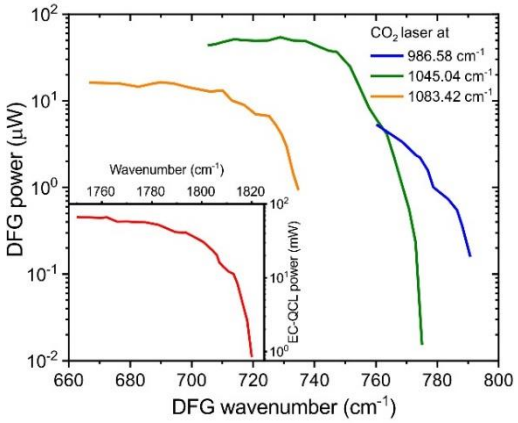

Fig. 2. Average power of the DFG laser at different wavenumbers of CO_2 laser. The CO_2 laser is operated at a repetition rate of 1 kHz with a duty cycle of 20 %. The inset shows the power of EC-QCL laser across its tuning wavenumber range.

Large and continuous tunability of the EC-QCL (pump source), as combined with the multi-line emission from the CO_2 gas laser (signal source), results in an effective wavenumber range for DFG laser (idler) from 666.54 cm^{-1} to 790.76 cm^{-1}. Figure 2 shows a few examples of the average power curves of the DFG laser at different signal wavenumbers. The shape of idler power curves follows the power curve of the pump laser shown in the inset of Fig. 2. The EC-QCL output power was measured before the input facet of the OP-GaAs crystal. The line-width of the DFG-based laser was found to be ~2.3 MHz. This corresponds to the width of the convolution between ECQCL and CO_2 emission spectra, which were directly measured against an ultra-narrow optical frequency comb.

2.2. Shock tube facility

The experiments presented in this paper were performed in the stainless steel, low-pressure shock-tube (LPST) facility at King Abdullah University of Science and Technology (KAUST). This LPST is made of a 9 m driver section and a 9 m driven section with an inner diameter of 14.22 cm. However, the length of the driver section can be varied to achieve the desired test time behind reflected shock waves.

We used the driver section in a length of 3 and 9 m to achieve a test time of about 1.5 and 8 ms, respectively. A polycarbonate diaphragm was used to separate the driven section from the driver one. For shock experiments, both the driven and driver sections were pumped down, and then the driven and driver sections were filled with the benzene/argon mixture and helium gas, respectively. Shock waves were generated when the helium pressure in the driver section was increased to a high-enough level to rupture the diaphragm. The speed of the incident shock was measured using a series of five piezoelectric PCB pressure transducers installed over the final 1.3 m of the driven section of the shock tube. The incident shock velocity was calculated by measuring the time interval between those five transducers. Standard one-dimensional shock-jump relations [29] embedded in the Frosh code [30] were used to calculate the reflected shock temperatures as well as pressures. The uncertainties in the calculated temperature and pressure are approximately ±0.7% and ±1%, respectively, with the major contribution coming from uncertainties in the incident shock speed and mixture composition. Further details about the shock tube facility can be found elsewhere [31,32].

3. Measurement principle and uncertainty

We used direct laser absorption spectroscopy to obtain the cross-section and the concentration of benzene. The absorption of a laser beam passed through a gas mixture can be related to the physical parameters of the gas as well as the experimental conditions *via* the Beer-Lambert relation:

$$\ln\left(\frac{I_t(\nu)}{I_0(\nu)}\right) \equiv -A(\nu,T,P) = -\sigma(\nu,T,P)nL \quad (1)$$

where I_t and I_0 are the transmitted and incident laser intensities, respectively, at a frequency (ν), A is the absorbance, σ is the absorption cross-section, T is the temperature, P is the pressure, n is the number density of the absorbing species, and L is the absorption path length. The relation between the mole fraction (x) of the absorbing species and the number density is:

$$n = \frac{N}{V} = \frac{xP}{k_B T} \quad (2)$$

where N is the number of absorbers in the volume $V$and k_B is the Boltzmann constant (k_B=1.38×10^{-23} J/K). From Eq. (1) and (2), one can get the relation between the absorption cross-section and the experimental parameters:

$$\sigma(\nu, T, P) = \frac{A(\nu,T,P)k_B T}{xpL} \quad (3)$$

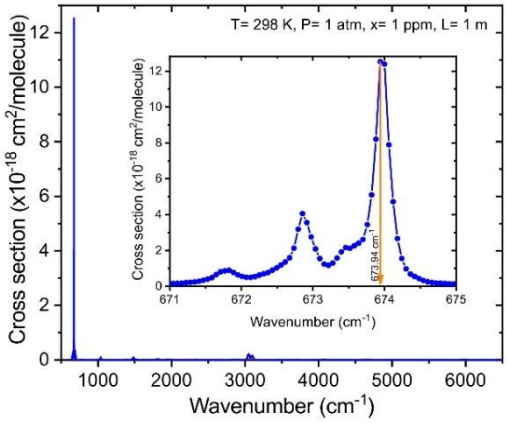

Fig. 3. Absorption cross-section of benzene in the MIR calculated from Eq. (3) using the absorbance values of PNNL. The inset is a zoom-in at the Q branch of benzene cross-section spectrum.

We used Eq. (3) to calculate the absorption cross-section of benzene using the absorbance values from PNNL (Pacific Northwest National Laboratory) database measured at 296 K and 1 atm [6]. Figure 3 shows the absorption cross-section over the IR spectrum between 600 cm^{-1} and 6500 cm^{-1}. Benzene has 20 fundamental vibrational bands across the infrared region; of these 10 vibrational motions are doubly-degenerate while 10 are non-degenerate. The strongest IR active band is the ν_{11} band (centered near 674 cm^{-1}), which is related to the C-H bending motions in benzene. This parallel band shows P, Q and R branch transitions over ~640–710 cm^{-1}. The highest cross-section in the ν_{11} band occurs at the peak of the Q branch. The inset of Fig. 3 is a zoom-in of the cross-section spectrum at the Q branch. The maximum value of the cross-section (at 298 K) is 12.53×10^{-18} cm^2/molecule at the wavenumber 673.94 cm^{-1}. This value is larger by a factor of ~80 compared to the commonly accessible vibrational band of benzene near 3100 cm^{-1} and it is furthermore greater by a factor of ~5 than the maximum value of the absorption cross-section of benzene in the ultraviolet spectral range (~2.44 ×10^{-18} cm^2/molecule at 39572 cm^{-1}) [28]

We tuned our DFG laser to 673.94 cm^{-1} by tuning the EC-QCL to 1752.73 cm^{-1} and the CO_2 gas laser to 1078.79 cm^{-1} as well as optimizing the position of the OP-GaAs crystal. The CO_2 gas laser repetition rate is set to 30 kHz with a 30% duty cycle. The DFG laser signal reflects the pulsed shape of the signal of the CO_2 gas laser, and consequently, the DFG laser has the aforementioned repetition rate.

To estimate the uncertainty in the absorption cross-section calculated from Eq. (3), we used the following formulae:

$$\frac{\delta\sigma}{\sigma} = \sqrt{\left(\frac{\delta A}{A}\right)^2 + \left(\frac{\delta T}{T}\right)^2 + \left(\frac{\delta x}{x}\right)^2 + \left(\frac{\delta P}{P}\right)^2} \tag{4}$$

where the uncertainty in the absorbance is

$$\frac{\delta A}{A} = \sqrt{\left(\frac{\delta I_t}{I_t}\right)^2 + \left(\frac{\delta I_0}{I_0}\right)^2} \tag{5}$$

We considered the uncertainty in I_t and I_0 as the standard deviation of the noise in each. The uncertainties in the temperature and pressure behind reflected shock waves are approximately ±0.7% and ±1%, respectively. The uncertainty in the mole fraction is 2%.

4. Pressure-dependent cross-section

We prepared a benzene/argon mixture with a benzene mole fraction of 341 ppm. The absorbance measurements were performed at room temperature (296 K) over a pressure range from 4.44 mbar to 1.158 bar. We used the driven section of the shock tube as a static cell with an absorption path-length of 14.22 cm. We simultaneously collected the signal on both detectors, D_1 and D_2, for 10 ms. Figure 4 (a) shows an example of the collected signals of D_1 and D_2 over 0.8 ms. A temporal delay of about 0.4 μs is considered between detectors' signals due to the difference in the optical passes of the DFG laser (See Fig.1 (b)). The R_{int} was first obtained with the shock tube at vacuum. Then, we filled the shock tube with benzene/argon mixture, and we applied the R_{int} to obtain the absorbance at different pressures. The D_2 signal was used to obtain the transmitted laser intensity, while the D1 signal was used to obtain the incident laser intensity. The fluctuation in the signals shown in Fig. 4 (a) is mainly

due to the detectors' noise; the peak-to-peak (P-P) amplitude of the irregular background noise signal is about 80 mV for D_2 and about 20 mV for D_1. To reduce the effect of the background noise, we used the P-P signal amplitude of both detectors to obtain the absorbance. Figure 4 (b) shows the measured P-P signal amplitude of transmitted, I_t, and incident, I_0, laser beams over 10 ms at a pressure of 0.2 bar. We used the standard deviation of the noise as the uncertainty in I_t and I_0.

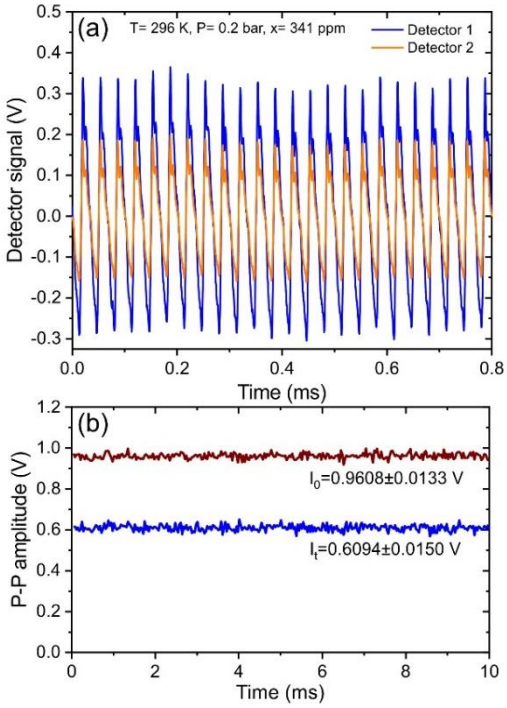

Fig. 4. (a) DFG laser signal on detector 1 and 2 collected at a pressure of 0.2 bar at RT. (b) Peak to peak signal amplitudes of transmitted (I_t) (multiplied with R_{int}) and incident (I_0) laser beams.

We used I_t and I_0 values to obtain the absorbance at each pressure. The obtained absorbance values as a function of the pressure are shown in Fig. 5(a). The absorbance proportionally increases with pressure, but at different increasing rates, i.e., the increasing rate (slope) is 0.92 bar^{-1} for the pressure below 0.27 bar, while it is 0.73 bar^{-1} for the higher pressures. The uncertainty in the absorbance value is calculated from Eq. (5). The relative absorbance uncertainty varies between 2% and 6.5%, with a tendency to increase with pressure. This is due to high benzene absorption at high pressures, resulting in a relatively low P-P signal amplitude of the transmitted laser beam and hence a significant uncertainty in its value.

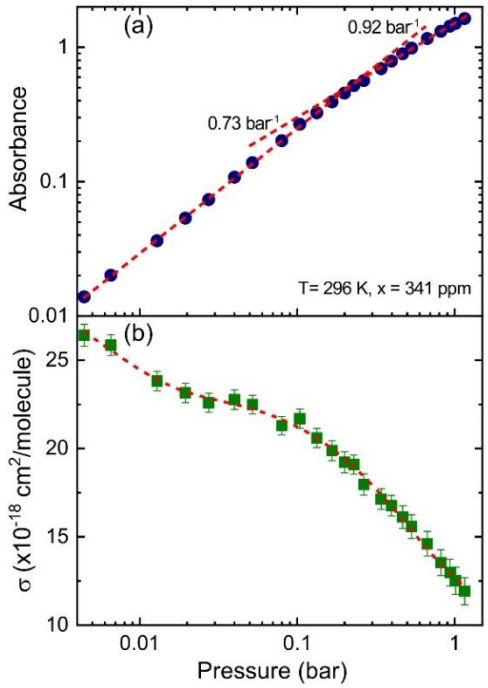

Fig. 5. (a) Absorbance and (b) absorption cross-section, at 673.94 cm^{-1}, as a function of the pressure at room temperature. The red dashed lines in (a) refer to the linear changes of the absorbance with the pressure. The red dashed line in (b) is a bi-exponential fitting of the data using Eq. (6).

Using the absorbance values, we applied Eq. (3) to determine the cross-sections of benzene at different pressures. Figure 4(b) shows the cross-section variation with the pressure. The cross-section exhibits evident pressure dependence with an obvious decrease with increasing pressure. The cross-section decreases gradually up to ~0.1 bar, and then it drops rapidly for a further increase in the pressure. These changes of cross-section with pressure are due to combined effects of changes in number density, line shape function, and line-center shift. The highest cross-section value of 26.41×10^{-18} cm^2/molecule is obtained at 4.44 mbar, which is more than twice higher than the cross-section value at atmospheric pressure. Pressure-dependent cross-section is fitted with the red dashed line in Fig. 5(b) using the following bi-exponential function:

$$\sigma(673.94\ cm^{-1}, 296\ K, P) = C_1 e^{\left(-\frac{P}{\tau_1}\right)} + C_2 e^{\left(-\frac{P}{\tau_2}\right)} + \sigma_0 \text{ [cm}^2\text{/molecule]} \quad (6)$$

where C_1=6.74976×10^{-18} cm^2/molecule, C_2=1.2702×10^{-17} cm^2/molecule, τ_1=6.17×10^{-3} bar, τ_2=0.536 bar, and σ_0= 1.0687×10^{-17} cm^2/molecule.

5. Temperature-dependent cross-section

We performed experiments behind reflected shock waves to determine the absorption cross-section of benzene at high temperatures. These experiments were performed over a wide range of temperatures between 553 and 1473 K with a variation in the pressure between 1.17 bar and 2.48 bar. The benzene mole fraction in its mixture with argon is varied between 0.048% and 1.18% to obtain optimal values of absorbance at various ranges of temperatures. The measured laser signals were averaged over 1 ms behind the reflected shock wave to determine the absorbance and hence the cross-section.

A representative shock tube experiment is shown in Fig. 6 for the determination of cross-section of benzene at 553 K and 1.6 bar. The green-highlighted part of the figure refers to the experimental condition before the shock arrival (room temperature), while the yellow-highlighted part refers to the experimental condition of 553 K behind the reflected shock wave. The transmitted, I_t, and incident, I_0, laser beam signals and the measured time-resolved pressure are shown in Fig. 6(b). The time zero at which the reflected shock arrived at the sidewall location was determined from the second step rise in the pressure signal. The incident shock region is not used for data analysis due to the lack of sufficient measurement points at our time resolution of 33 μs.

The offset in the transmitted laser signal (detector 1) behind the incident and reflected shock waves is due to the thermal radiation during the shock experiment. This radiation just causes a shift in the transmitted laser signal, but it does not affect the peak-to-peak (P-P) laser amplitude. The offset in this signal is subtracted when P-P amplitude is determined. Figure 6(b) shows the time-resolved P-P signal amplitudes of transmitted, I_t, and incident, I_0, laser beams and the pressure time-history. The P-P amplitude of transmitted laser beam, I_t, dramatically increased behind reflected shock wave due primarily to the large jump in the number density. We used the amplitudes of I_t and I_0 to obtain the absorbance for each shock experiment and then used the obtained absorbance value to calculate the absorption cross-section from Eq. (3). The uncertainty in the cross-section is determined from Eq. (4).

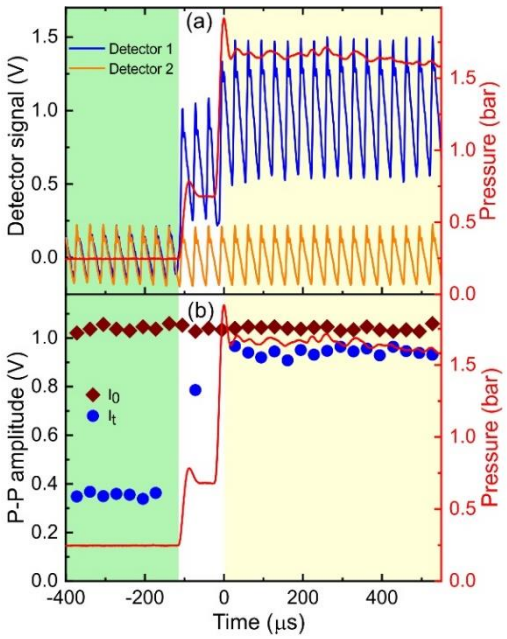

Fig. 6. (a) Detector signals of transmitted and incident laser beams, before the shock at room temperature (green-highlighted) and behind reflected shock wave at 553 K (yellow-highlighted). (b) Time-resolved peak to peak (P-P) amplitudes of transmitted (I_t) and incident (I_0) laser signal. Pressure (red) is also shown in both panels.

The blue circles in Fig. 7 show the absorption cross-section of benzene as a function of temperature. The cross-section decreases with increasing temperature. This shows that the selected wavelength corresponds to a cumulative effect of closely-spaced low E" Q-branch rotational lines. The cross-section is about 0.11×10^{-18} at 1473 K which is less by about 100 times than its value at room temperature. The best fit to the experimental results of the pressure-dependent cross-section is done using a bi-exponential function, as shown in red dashed line in Fig. 7. Due to the weak pressure dependence of the cross-section on pressure at high temperatures, we considered the cross-section as a function of temperature only during the fitting process. The bi-exponential function used to simulate the experimental results is:

$$\sigma(673.94\ cm^{-1}, T, 1.17-2.48\ \text{bar}) = B_1 e^{\left(-\frac{T}{\gamma_1}\right)} + B_2 e^{\left(-\frac{T}{\gamma_2}\right)} + \sigma_0\ [\text{cm}^2/\text{molecule}] \quad (7)$$

where $B_1=1.71\times10^{-16}$ cm^2/molecule, $B_2=1.02\times10^{-18}$ cm^2/molecule, $\gamma_1=109.34$ K, $\gamma_2=558.43$ K, and $\sigma_0=4.99\times10^{-20}$ cm^2/molecule.

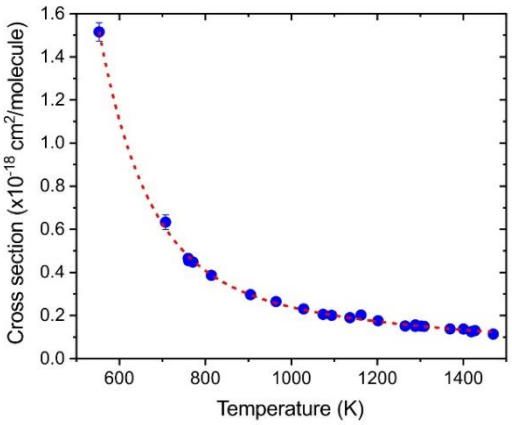

Fig. 7. Absorption cross-section, at 673.94 cm^{-1}, as a function of the temperature. The red dashed line is the best fitting of the data using the bi-exponential function of Eq. (7).

6. Application to reactive experiments

The main objective of this new diagnostic method is to investigate benzene chemistry, particularly the formation and consumption kinetics of benzene at combustion-relevant conditions. As a representative demonstration, we applied this laser system to monitor benzene formation from propargyl radicals in shock tube experiments. A mixture of 4.6% propargyl iodide (C_3H_3I) in argon was shock heated to reach reflected shock temperature and pressure of 961 K and 1.36 bar, respectively. The absorbance of benzene was obtained according to the procedure illustrated in the previous sections. Thereafter, the obtained absorbance was converted to mole fraction with the help of absorption cross-section calculated from Eq. (7). Benzene mole fraction (blue trace) is plotted in Fig. 8 along with the measured pressure trace (red trace). Figure 8 also shows the simulated benzene mole fraction using the benzene model from Miller and Klippenstein [33] and the propargyl iodide sub-mechanism from Tranter et al. [34]. Under our experimental condition, C_3H_3I decomposes within $\sim$0.2 ms, yielding propargyl radical. According to the calculations of Miller and Klippenstein [33], propargyl recombination quickly forms fulvene and benzene. Fulvene is not stable, and it will slowly isomerize to benzene. Our measured benzene profile well captured this isomerization process. For this particular case, the agreement between experiment and model prediction is very good. However, this is not to be expected at other reaction conditions since our understanding of benzene / PAH chemistry is far from being perfect. The new diagnostic developed here will prove to be highly beneficial for such investigations.

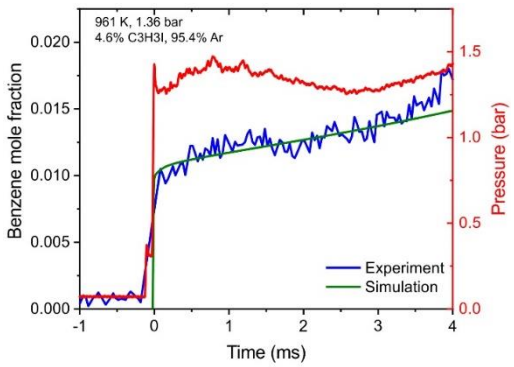

Fig. 8. Time-resolved measurement of benzene mole fraction at reflected shock conditions of 961 K and 1.36 bar. Pressure trace is also shown (right axis). Benzene simulation is based on a cumulative model based on Refs. [33,34].

7. Summary and outlook

We have reported the development and application of a new mid-IR laser diagnostic for benzene sensing. The chosen wavelength region has not been used previously for high-temperature investigations of benzene due to the non-availability of commercial laser sources. Our diagnostic is based on the difference-frequency-generation process between an EC-QCL and a CO_2 gas laser in a nonlinear, orientation-patterned GaAs crystal. The laser system emits in the mid-IR region between 666.54 and 790.76 cm^{-1}. The laser was tuned to the peak of the Q-branch transition near 673.94 cm^{-1}. Room temperature measurements showed that the benzene cross-section is quite sensitive to pressure. We performed experiments behind reflected shock waves to determine the absorption cross-section of benzene over 553 K–1473 K and 1.17–2.48 bar. Our results show that the cross-section of benzene is about 0.11×10^{-18} at 1473 K, which is considerably smaller than the room temperature value. Future work will, therefore, investigate other wavelengths of benzene in this region, which may exhibit decreased temperature dependence and/or larger cross-section at high temperatures. The new diagnostic was also demonstrated in reactive shock tube experiments of benzene formation from propargyl iodide. In the future, this diagnostic will be combined with a mid-IR acetylene diagnostic and a visible scattering diagnostic [35] to investigate PAH and soot formation processes.

Acknowledgements

Research reported in this publication was funded by the Office of Sponsored Research and King Abdullah University of Science and Technology (KAUST).

References

[1] C.S. Goldenstein, R.M. Spearrin, J.B. Jeffries, R.K. Hanson, Infrared laser-absorption sensing for combustion gases, Prog. Energy Combust. Sci. 60 (2017) 132–76.

[2] R.K. Hanson, D.F. Davidson, Recent advances in laser absorption and shock tube methods for studies of combustion chemistry, Prog. Energy Combust. Sci. 44 (2014) 103–14.

[3] R.K. Hanson, Applications of quantitative laser sensors to kinetics, propulsion and practical energy systems, Proc. Combust. Inst. 33 (1) (2011) 1–40.

[4] E. Tomita, N. Kawahara, A. Nishiyama, M. Shigenaga, In situ Measurement of Fuel Concentration of Hydrocarbon near Spark Plug in an Engine Cylinder by 3.392 μm Infrared Laser Absorption Method (Application to Actual Engine), Nippon Kikai Gakkai Ronbunshu, B Hen/Transactions Japan Soc. Mech. Eng. Part B 70 (690) (2004) 518–24.

[5] J.B. Jeffries, C. Schulz, D.W. Mattison, M.A. Oehlschlaeger, W.G. Bessler, T. Lee, et al., UV absorption of CO2 for temperature diagnostics of hydrocarbon combustion applications, Proc. Combust. Inst. 30 (1) (2005) 1591–9.

[6] S.W. Sharpe, T.J. Johnson, R.L. Sams, P.M. Chu, G.C. Rhoderick, P.A. Johnson, Gas-phase databases for quantitative infrared spectroscopy, Appl. Spectrosc. 58 (12) (2004) 1452–61.

[7] M. Razeghi, W. Zhou, S. Slivken, Q.-Y. Lu, D. Wu, R. McClintock, Recent progress of quantum cascade laser research from 3 to 12 μm at the Center for Quantum Devices [Invited], Appl. Opt. 56 (31) (2017) H30.

[8] M.S. Vitiello, G. Scalari, B. Williams, P. De Natale, Quantum cascade lasers: 20 years of challenges, Opt. Express 23 (4) (2015) 5167.

[9] P. Rauter, F. Capasso, Multi-wavelength quantum cascade laser arrays, Laser Photonics Rev. 9 (5) (2015) 452–77.

[10] C. Gaida, M. Gebhardt, T. Heuermann, F. Stutzki, C. Jauregui, J. Antonio-Lopez, et al., Watt-scale super-octave mid-infrared intrapulse difference frequency generation, Light Sci. Appl. 7 (1) (2018).

[11] I.T. Sorokina, K.L. Vodopyanov, Solid-state mid-infrared laser sources, Topics in Applied Physics, 2003, p. 263.

[12] R. Sivaramakrishnan, K. Brezinsky, H. Vasudevan, R.S. Tranter, A shock-tube study of the high-pressure thermal decomposition of benzene, Combust. Sci. Technol. 178 (1–3) (2006) 285–305.

[13] B. Shukla, K. Tsuchiya, M. Koshi, Novel products from C6H5 + C6H 6/C6H5 reactions, J. Phys. Chem. A 115 (21) (2011) 5284–93.

[14] Pah Growth and Soot Formation in the Pyrolysis of Acetylene and Benzene At High Temperatures and Pressures : Modeling (2000) 1605–12.

[15] H. Richter, T.G. Benish, O.A. Mazyar, W.H. Green, J.B. Howard, Formation of polycyclic aromatic hydrocarbons and their radicals in a nearly sooting premixed benzene flame, Proc. Combust. Inst. 28 (2) (2000) 2609–18.

[16] Y. Rezgui, M. Guemini, Benzene combustion: A detailed chemical kinetic modeling in laminar flames conditions, Kinet. Catal. 55 (3) (2014) 278–86.

[17] C.P. Rinsland, V.M. Devi, T.A. Blake, R.L. Sams, S. Sharpe, L. Chiou, Quantitative measurement of integrated band intensities of benzene vapor in the mid-infrared at 278, 298, and 323 K, J. Quant. Spectrosc. Radiat. Transf. 109 (15) (2008) 2511–22.

[18] J.C. Lee, D.E. Lee, T. Schultz, High-resolution rotational Raman spectroscopy of benzene, Phys. Chem. Chem. Phys. 21 (6) (2019) 2857–60.

[19] J. Kauppinen, P. Jensen, S. Brodersen, Determination of the B , Constant, J. Mol. Spectrosc. 83 (1980) 161–74.

[20] J. Berger, V. V. Pustogov, Monitoring of benzene in the 10 μm and 14 μm region, Infrared Phys. Technol. 37 (1) (1996) 163–6.

[21] W. Chen, F. Cazier, F. Tittel, D. Boucher, Measurements of benzene concentration by difference-frequency laser absorption spectroscopy, Appl. Opt. 39 (33) (2000) 6238.

[22] M.T. Parsons, I. Sydoryk, A. Lim, T.J. McIntyre, J. Tulip, W. Jäger, et al., Real-timemonitoring of benzene, toluene, and p-xylene in a photoreaction chamber with a tunable mid-infrared laser and ultraviolet differential optical absorption spectroscopy, Appl. Opt. 50 (4) (2011).

[23] I. Sydoryk, A. Lim, W. Jäger, J. Tulip, M.T. Parsons, Detection of benzene and toluene gases using a midinfrared continuous-wave external cavity quantum cascade laser at atmospheric pressure, Appl. Opt. 49 (6) (2010) 945–9.

[24] J.D. Jeffers, C.B. Roller, K. Namjou, M.A. Evans, L. McSpadden, J. Grego, et al., Real-Time Diode Laser Measurements of Vapor-Phase Benzene, Anal. Chem. 76 (2) (2004) 424–32.

[25] C.B. Hirschmann, S. Sinisalo, J. Uotila, S. Ojala, R.L. Keiski, Trace gas detection of benzene, toluene, p-, m- and o-xylene with a compact measurement system using cantilever enhanced photoacoustic spectroscopy and optical parametric oscillator, Vib. Spectrosc. 68 (2013) 170–6.

[26] J. Cousin, W. Chen, D. Bigourd, M. Fourmentin, S. Kassi, Telecom-grade fiber laser-based difference-frequency generation and ppb-level detection of benzene vapor in air around 3 μm, Appl. Phys. B Lasers Opt. 97 (4) (2009) 919–29.

[27] S.H. Bauer, C.F. Aten, Absorption spectra of polyatomic molecules at high temperatures. II. Benzene and perfluorobenzene. Kinetics of the pyrolysis of benzene, J. Chem. Phys. 39 (5) (1963) 1253–60.

[28] T. Etzkorn, B. Klotz, S. Sørensen, I. V. Patroescu, I. Barnes, K.H. Becker, et al., Gas-phase absorption cross sections of 24 monocyclic aromatic hydrocarbons in the UV and IR spectral ranges, Atmos. Environ. 33 (4) (1999) 525–40.

[29] J. N. Bradley, Shock Waves in Chemistry and Physics, Methuen, London, 1962, .

[30] M.F. Campbell, D.R. Haylett, D.F. Davidson, R.K. Hanson, AEROFROSH: a shock condition calculator for multi-component fuel aerosol-laden flows, Shock Waves 26 (4) (2016) 429–47.

[31] S.M. Sarathy, T. Javed, F. Karsenty, A. Heufer, W. Wang, S. Park, et al., A comprehensive combustion chemistry study of 2,5-dimethylhexane, Combust. Flame 161 (6) (2014) 1444–59.

[32] M.B. Sajid, E. Es-Sebbar, T. Javed, C. Fittschen, A. Farooq, Measurement of the rate of hydrogen peroxide thermal decomposition in a shock tube using quantum cascade laser absorption near 7.7 μm, Int. J. Chem. Kinet. 46 (5) (2014) 275–84.

[33] J.A. Miller, S.J. Klippenstein, The recombination of propargyl radicals and other reactions on a C6H6 potential, J. Phys. Chem. A 107 (39) (2003) 7783–99.

[34] R.S. Tranter, X. Yang, J.H. Kiefer, Dissociation of C3H3I and rates for C3H3 combination at high temperatures, Proc. Combust. Inst. 33 (1) (2011) 259–65.

[35] U. KC, M. Beshir, A. Farooq, Simultaneous measurements of acetylene and soot during the pyrolysis of ethylene and benzene in a shock tube, Proc. Combust. Inst. 36 (1) (2017) 833–40.

List of Figure Captions

Fig. 1. Schematic drawing of (a) the DFG laser setup and (b) the cross-section of the shock tube. EC-QCL: external-cavity quantum cascade laser; OI: optical isolator; CM: concave mirror; BC: beam combiner; PM: parabolic mirror; M: mirror (flat); OP-GaAa: orientation-patterned GaAs crystal; LF: long-pass filter; BS: beam splitter; D: detector.

Fig. 2. Average power of the DFG laser at different wavenumbers of CO_2 laser. The CO_2 laser is operated at a repetition rate of 1 kHz with a duty cycle of 20 %. The inset shows the power of EC-QCL laser across its tuning wavenumber range.

Fig. 3. Absorption cross-section of benzene in the MIR calculated from Eq. (3) using the absorbance values of PNNL. The inset is a zoom-in at the Q branch of benzene cross-section spectrum.

Fig. 4. (a) DFG laser signal on detector 1 and 2 collected at a pressure of 0.2 bar at RT. (b) Peak to peak signal amplitudes of transmitted (I_t) (multiplied with R_{int}) and incident (I_0) laser beams.

Fig. 5. (a) Absorbance and (b) absorption cross-section, at 673.94 cm^{-1}, as a function of the pressure at room temperature. The red dashed lines in (a) refer to the linear changes of the absorbance with the pressure. The red dashed line in (b) is a bi-exponential fitting of the data using Eq. (6).

Fig. 6. (a) Detector signals of transmitted and incident laser beams, before the shock at room temperature (green-highlighted) and behind reflected shock wave at 553 K (yellow-highlighted). (b) Time-resolved peak to peak (P-P) amplitudes of transmitted (I_t) and incident (I_0) laser signal. Pressure (red) is also shown in both panels.

Fig. 7. Absorption cross-section, at 673.94 cm^{-1}, as a function of the temperature. The red dashed line is the best fitting of the data using the bi-exponential function of Eq. (7).

Fig. 8. Time-resolved measurement of benzene mole fraction at reflected shock conditions of 961 K and 1.36 bar. Pressure trace is also shown (right axis). Benzene simulation is based on a cumulative model based on Refs. [33,34].